ASTRONOMY & ASTROPHYSICS
SUPPLEMENT SERIES

*Astron. Astrophys. Suppl. Ser.* **94**, 13-35 (1992)



# High-frequency radio continuum observations of low-luminosity radio galaxies

## I. A sample of sources with angular sizes > 4′

L. Gregorini[1], U. Klein[2], P. Parma[1], R. Schlickeiser[2] and R. Wielebinski[2]

[1] Istituto di Radioastronomia, Via Irnerio 46, 40126 Bologna, Italy
[2] Max-Planck-Institut für Radioastronomie, Auf dem Hügel 69, 5300 Bonn 1, Germany

*Received May 29; accepted July 24, 1991*

**Abstract.** — A sample of 10 low-luminosity radio galaxies with angular size greater than 4 arcmin has been observed at 10.6 GHz using a new multi-feed receiver system installed in the secondary focus of the Effelsberg 100-m telescope. Sensitive maps of the total and linearly polarized radio emission allow us to study the large-scale distribution of the synchrotron radiation and its spectral behaviour which at short cm wavelengths cannot be measured with interferometers. Since Faraday rotation is almost negligible at this wavelength, the intrinsic projected large-scale magnetic field is directly mapped by these observations. Studies of the depolarization and Faraday rotation in radio galaxies are greatly improved by incorporating observations at such wavelengths. In general, the degree of polarization at 10.6 GHz is found to be higher in the outer parts (e.g. lobes) than in the inner parts of the sources, and it is significantly higher over most of the sources than what is measured at lower frequencies (1.4 GHz). The magnetic field orientation seems related to the morphologies of the sources. Except for one case, which is a relic radio galaxy, the integrated high-frequency spectra do not show any signs of steepening and hence particle aging.

**Key words:** radio galaxies – polarization – magnetic fields

## 1. Introduction.

An extensive study of two complete samples of 105 low-luminosity radio galaxies, selected from the B2 catalogue, was carried out in recent years (de Ruiter *et al.* 1990, and references therein). Observations of these radio galaxies were made with different radio telescopes between 408 MHz and 5 GHz. The samples were studied with different configurations of the VLA at 1.4 GHz (Fanti *et al.* 1987, and references therein), and at 5 GHz for a minority of sources (Morganti *et al.* 1987; Giovannini *et al.* 1988, Feretti, *et al.* 1990 and references therein). The most extended sources were observed with the WSRT at 5 GHz and/or at 1.4 GHz and 0.6 GHz (Parma *et al.* 1985, and references therein). Furthermore, for 37 sources integral source properties measured with the Effelsberg radio telescope at 2.7 GHz are available (Parma & Weiler 1981).

All of the information on the morphology, spectral index and polarization properties of low-luminosity radio galaxies were collected in an intermediate frequency range, and some of the basic questions to be elucidated with such measurements are still unanswered, such as the problem of whether the Faraday rotation in such radio sources is primarily intrinsic or whether it occurs in a magnetoionic foreground sheet. We therefore decided to extend the study of their characteristics towards higher frequencies. From the two complete samples of low-luminosity radio galaxies we selected those sources with an angular size greater than 4 arcmin in order to have adequate resolution, and we observed them at 10.6 GHz using the 100-m Effelsberg radio telescope. So far, high-frequency investigations of radio galaxies which are sensitive to the large-scale components have been made by Kronberg *et al.* (1986) and by Andernach *et al.* (1992).

In Section 2 we describe the observations and the data reduction procedure. In Section 3 we present the results (radio images in total and polarized intensity, integral properties) and briefly discuss these, and in Section 4 a brief summary is given. A detailed comparison of the present measurements with those at lower frequencies will be presented elsewhere.

## 2. Observations and data reduction.

We refer to Fanti *et al.* (1987) for a detailed description of the samples and of their selection criteria. For the present study we have selected 10 radio galaxies with angular sizes exceeding 4′. This ensured sufficient spatial

*Send offprint requests to*: U. Klein

resolution for a useful high-frequency study and, at the same time, provides a first test of the performance of the new 10.6 GHz receiver system of the Effelsberg 100-m telescope for such objects.

The observations have been carried out between January and May 1990 using the new 10.6 GHz ($\lambda$2.8 cm) 8-channel receiver system installed in the secondary focus of the 100-m telescope of the MPIfR. This system consists of 2 modules, each hosting 2 feeds and the subsequent RF sections. RF amplification is achieved by very stable HEMTs. Each feed is followed by a circular polarization polarizer to provide two channels with left and right circularly polarized voltages. These are mixed with a local oscillator signal to provide IF voltages $V_L$ and $V_R$. The two circular polarizations are detected to provide total power signals $V_L^2$ and $V_R^2$, assuming that the received signal has zero circular polarization. The other halves of the two signals are fed into an IF polarimeter to be processed in a quadrature network such as to provide $V_L \cdot V_R \cdot \cos\phi$ and $V_L \cdot V_R \cdot \sin\phi$, where $\phi$ is the relative phase shift of the two circularly polarized components. These latter two powers are proportional to Stokes parameters $Q$ and $U$, which fully describe the linear polarization of the incoming wave. The four feeds can now be used in connection with the so-called software beam-switching technique (Morsi & Reich 1986) to provide power differences between any pair of horns, thus efficiently cancelling out any atmospheric perturbations imposed on the signal. The great advantage of this technique as compared to previous hardware switching (see e.g. Klein & Emerson 1981) or correlation systems (see e.g. Gioia *et al.* 1982) is the relatively simple design and the fact that one is always "on source". The basic observing mode of such a multi-beam system when mapping extended radio sources was described by Emerson *et al.* (1979). Since all 4 horns have their own polarimeters, this new receiving system is a major improvement compared to the previous one concerning the sensitivity both, in total power as well as in polarized intensity. Note that this sensitivity relies heavily on the stability of the HEMT amplifiers. The basic telescope properties and characteristics of the receiving system are compiled in Table 1.

TABLE 1. *Receiver and telescope parameters.*

| | |
|---|---|
| Centre frequency | 10.55 GHz |
| Bandwidth | 300 MHz |
| System temperature | 50 K |
| Number of feeds | 4 |
| Number of receiver channels | 8 (4 LHC, 4 RHC) |
| Number of polarimeters | 4 |
| Number of channels recorded | 16 |
| Available beam throws | 2'.92, 4'.89, 8'.89 |
| | 11'.81, 13'.78, 16'.70 |
| Aperture efficiency | 42% |
| Main beam solid angle | $1.3 \cdot 10^{-7}$ sr |
| $T_b/S$ | 2.25 K/Jy |
| Highest sidelobe | −15 dB |
| Half power beam width | 69″ (circular) |

After detection the signals are processed by an A/D converter after which they are fed into the on-line computer.

The maps which have to be scanned in an azimuth-elevation coordinate system in order to take full advantage of the multi-beam mapping technique (see Emerson *et al.* 1979) must have sufficient lengths (in the scanning direction) to account for the largest beam throw (~17′). Each horn delivers 4 maps of the field covered (2× Stokes $I$, $Q$ and $U$). Since the feeds remain fixed in the secondary focus, the $Q$ and $U$ output has to be corrected for the change in parallactic angle. This is done in the tabscan stage, prior to the map making. In the first map stage, the calibration scale of all individual channels is adjusted to account for gain differences in the receiver systems. The corresponding factors have been determined in the course of extensive test measurements using strong point sources (Reich, priv. comm.).

After adjusting the calibration scales of all individual channels the two total power maps from each horn are averaged. The resulting 6 differential images, obtained by subtracting the total power maps of all possible horn pairs, are largely free from atmospheric fluctuations and have to be restored using the method of Emerson *et al.* (1979) to provide the equivalent single-beam maps. The next step involves a left-to-right inversion of the maps in order to account for the different sense of right ascension and azimuth, as well as shifting the restored single-beam images onto the map centres corresponding to the optical axis of the linear horn array. It is at this stage that the $I$, $Q$ and $U$ maps from all horns can be averaged to yield mean $I$, $Q$ and $U$ images of one coverage. The final step transforms the azimuth-elevation maps into equatorial coordinates. If several such coverages have been obtained, they can be averaged to improve the signal-to-noise ratio, utilizing in particular a Fourier filter technique to remove residual scanning noise (see Emerson & Gräve 1988). Further editing of the data (e.g. to remove interference spikes) can be done preferentially during the initial map stage. Essentially all of the software used for the data reduction is based on the standard NOD2 package (Haslam 1974).

Each source was mapped by scanning a field of size $(\theta_s + 23') \times (\theta_s + 2')$, where $\theta_s$ is the maximum source extent, in azimuth and elevation respectively, with the scanning direction in azimuth and a scan separation of 20″. A drive rate of 40′ per minute ensured minimum baseline drifts during each scan. Calibration was achieved by mapping the flux density standards 3C 123, 3C 138, 3C 147, 3C 286, 3C 295, and NGC 7027 in the same way as the radio galaxies. The flux density scale is that of

Baars *et al.* (1977), with the caveat that some of the sources (except 3C 286 and 3C 295) have slightly changed since then (Ott 1991). Pointing checks and focussing have been performed by frequently cross-scanning the above sources and 3C 48. Calibration of the polarization parameters has been achieved using the maps of 3C 123, 3C 138, and 3C 286 for which we have adopted polarization degrees and angles at 10.6 GHz of 3.8%, 11.9%, 11.6% and 179°, 173°and 36°, respectively. The instrumental polarization obtained from the map of NGC 7027 is $\lesssim$1%. The corresponding responses of Stokes $Q$ and $U$ to this source are displayed in Figure 1.

Up to a dozen coverages have been obtained for our target sources, some of which had to be rejected because of strong interference or imperfect weather cancellation. Table 2 summarizes the observations.

TABLE 2. *Observing details.*

| Source | Obs. dates (1990) | Number of coverages used | | rms noise [mJy/b.a.] | |
|---|---|---|---|---|---|
| | | total power | polarization | total power | polarization |
| 0034+25 | Jan. 6,30; Feb. 4 | 6 | 6 | 1.2 | 0.7 |
| 0326+39 | Jan. 6,7,10; Feb. 5 | 6 | 6 | 1.4 | 1.0 |
| 0828+32 | Jan. 6,7,10,30; Feb. 5; Mar. 28 | 12 | 10 | 1.4 | 0.6 |
| 0844+31 | Jan. 8,10,30; Feb. 5; Mar. 27 | 10 | 6 | 1.0 | 0.7 |
| 0915+32 | Jan. 8,30; Feb. 5; Mar. 27,28 | 12 | 12 | 1.0 | 0.5 |
| 0924+30 | Jan. 8,11; Feb. 5; Mar. 28 | 7 | 7 | 1.1 | 0.7 |
| 1116+28 | Jan. 8,11,31; Mar. 27 | 8 | 8 | 1.1 | 0.7 |
| 1321+31 | Jan. 11, Feb. 2; Mar. 29 | 8 | 9 | 1.2 | 0.9 |
| 1615+35 | Jan. 6,7,31; Mar. 28 | 6 | 6 | 1.4 | 0.9 |
| 1827+32 | Jan. 7,31; Feb. 2; Mar. 29 | 11 | 8 | 1.0 | 0.7 |

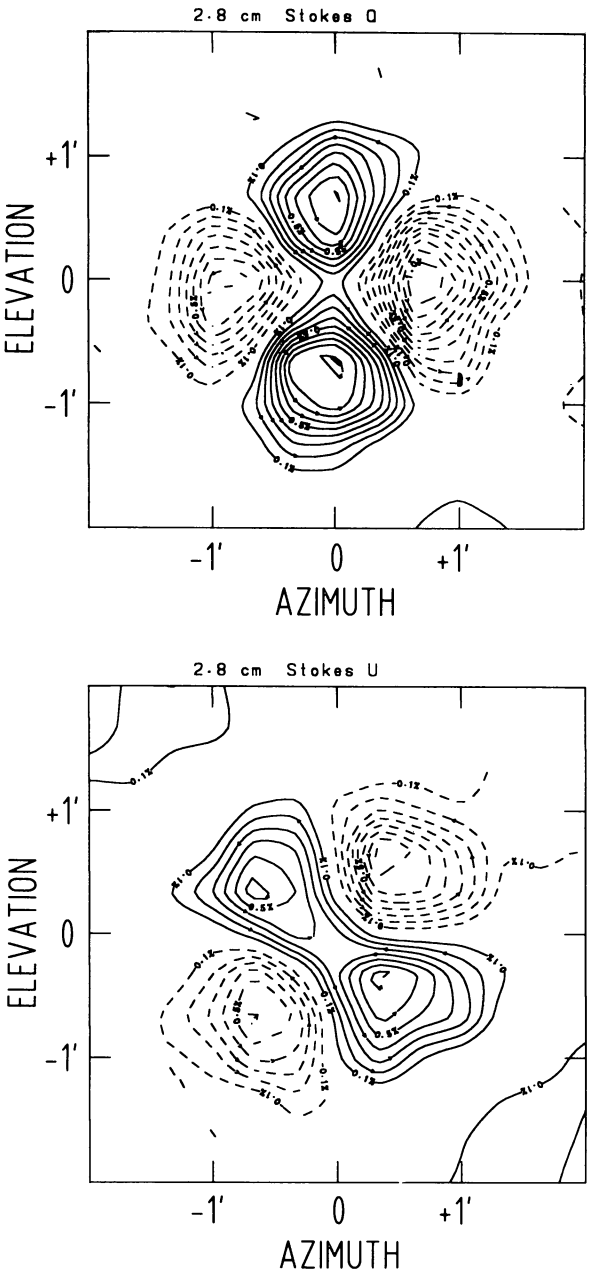


FIGURE 1. Instrumental polarization pattern obtained by mapping NGC 7027. a) Stokes parameter $Q$; b) Stokes parameter $U$. Contours are 0.1%, 0.2%, ... (solid contours), −0.1%, −0.2%, ... (dashed contours). Units are relative to the maximum of Stokes parameter I.

## 3. Results and discussion.

In this section we present the maps of the present sample of low-luminosity radio galaxies. Concerning the positions, redshifts, and optical magnitudes of the host galaxies we refer to the tables in Colla *et al.* (1975) and in Fanti *et al.* (1978). For each object, a map of its total as well as of its linearly polarized emission at 10.6 GHz is presented, with a brief description of the most salient features. A preliminary comparison is made with low-frequency VLA and WSRT images. Contour levels are compiled in Table 3. Integral properties deduced from the present measurements are summarized in Table 4, with the B2 name of the sources given in column 1. Column 2 of this table lists the total 10.6 GHz flux densities and their estimated errors. These have been obtained by integrating the maps of the calibration sources and the target sources in circular or elliptical rings such as to fit the source morphology as good as possible. The errors reflect mainly the uncertainties in the map zero levels. Column 3 gives the polarized flux densities obtained by integrating the $Q$ and $U$ maps in the same way and by computing $I_p = (Q^2 + U^2)^{1/2}$. These integrations also resulted in total polarization degrees and angles (columns 4 and 5). In column 6 and 7 the monochromatic radio luminosity at 10.6 GHz and the 5 GHz core luminosities (taken by Giovannini *et al.* 1988) are given respectively. The computed values are based

TABLE 3. *In all contour plots the hatched area in the lower left indicates the beam size (69″), while the bar at the top right calibrates the* **E***-vectors which are superimposed. In the total power maps the* **E***-vectors have lengths proportional to the polarized flux density per beam area, while those in the polarization maps have lengths proportional to the degree of polarization.*

| Figure | Contour levels [mJy/beam area] |
|---|---|
| 2a | 3,5,7,9,11 |
| 2b | 1,1.5 |
| 3a | 3,6,9,12,15,20,25,30,40,50,60,70,80 |
| 3b | 2,3,4,5,6 |
| 4a | 3,6,8,10,12,15,20,30,40,50,60,70,80,90,100 |
| 4b | 2,3,4,5,6,7,8,9,10,12,14,16,18,20 |
| 5a | 3,6,9,12,15,20,30,40,50,60,70 |
| 5b | 1.5,2,3,4.5 |
| 6a | 2,4,6,8,10,14,18,22,26,30,34 |
| 6b | 1,1.5,2,2.5,3,3.5,4 |
| 7a | 3,6,9,12,15,20,30,40,50 |
| 7b | 1,2,3,4 |
| 8a | 3,6,9,12,15,20,25,30,35,40,45 |
| 8b | 2,4,6,8,10,12,14,16 |
| 9a | 3,6,9,12,15,20,25,30,40,50,60,70,80,90,100, 110,120,130 |
| 9b | 2,3,4,5,6,7,8,9,10 |
| 10a | 2,4,6,8,10,15,20,25,30 |
| 10b | 1,1.5 |

on a Hubble constant of $H_0 = 100$ km s$^{-1}$ Mpc$^{-1}$ and assuming $q_0 = 1$.

Integral source properties, some of which are comprised in Table 4, will be discussed at the end of this section.

### 3.1. B2 0034+25.

Our maps of the total and linearly polarized intensity at 10.6 GHz of this wide-angle tail (WAT) source (see Ekers *et al.* 1981, de Ruiter *et al.* 1986) are displayed in Figures 2a and b. The southern tail is still visible at this frequency. The degree of linear polarization reaches ~30%, the average being 5.4±2.0%. The integral polarization angle is 108°±11°, close to the value of 117°±7° found by Parma & Weiler (1981) at 2.7 GHz. Together with the angle of 125° at 1.4 GHz (Ekers *et al.* 1981), a rotation measure of about +7 rad m$^{-2}$ results, the three values being consistent within the errors.

The integrated spectral index between 1.4 GHz and 10.6 GHz is the same as that at lower frequencies (Ekers *et al.* 1981), with $\alpha = -0.62 \pm 0.01$ ($S_\nu \sim \nu^\alpha$).

### 3.2. B2 0326+39.

This source has recently been studied thoroughly between 0.6 and 5 GHz by Bridle *et al.* (1991) using the VLA and the WSRT. The "S"-type asymmetry which was already noted by Ekers *et al.* (1981) shows up in our 10.6 GHz map (Fig. 3a) only marginally if anything. At this frequency the brightness of the core has become stronger compared to the lobes, corroborating the flat spectral index found by Bridle *et al.* (1991).

Figure 3b displays the map of the linearly polarized brightness of B2 0326+39. The degree of linear polarization is highest at the outer edges of the lobes, exceeding some 30% locally. In the lobe centres we derive between 6% and 10% linear polarization. Some depolarization at 10.6 GHz is indicated there, comparing our measurements with those of Bridle *et al.* (1991). This is obviously the result of beam depolarization, owing to the non-uniform magnetic field structure within the lobes. In the central region we find ~10% polarization, indicating some marginal depolarization at lower frequencies. Bridle *et al.* (1991) find between 5% and 12% polarization for the central (~40″) component.

The distribution of polarization angles indicates significant Faraday rotation between 1.4 GHz and 10.6 GHz if we compare the map in Figure 3b with that of Bridle *et al.* (1991). The rotation measures determined by Bridle *et al.* are consistent with our polarization angles. The integral position angle at 10.6 GHz is $\chi = 118° \pm 8°$, and Parma & Weiler (1981) reported $\chi = 165° \pm 2°$ at 2.7 GHz. This would imply a rotation measure of +73 rad m$^{-2}$, significantly more than the typical values found by Bridle *et al.* across this source. However, the measurements of Parma and Weiler were made with a 4′.5 beam so that they probably did not pick up the whole flux. Rotating our polarization vectors by 90°, we find a good correspondence between the magnetic field orientation at 10.6 GHz and the magnetic field model sketched by Bridle *et al.* (1991). Using our data, we shall be able to refine that model.

Our total flux density at 10.6 GHz (Tab. 4) does not show any break in the spectrum (Fig. 11b), with a spectral index of $\alpha = -0.70 \pm 0.01$ being maintained from 408 MHz through 10.6 GHz.

### 3.3. B2 0828+32.

This intriguing source shows two lobe systems at lower frequencies (Parma *et al.* 1985, Machalski & Condon 1985), probably reminiscent of precession of the central machine which powers the radio lobes. Our 10.6 GHz map shown in Figure 4a shows the main lobes, while the steep-spectrum secondary lobes which run roughly north-south are only marginally indicated, owing to the limited dynamic range of our map which is disturbed by residual scanning effects. Nevertheless, it can be seen that the southern extension of

TABLE 4. *Integral source properties at 10.6 GHz.*

| Source | $S_{tot}$ [mJy] | $S_p$ [mJy] | p [%] | $\chi$ [°] | log $P_{10.7}$ [W Hz$^{-1}$] | log $P_5^{core}$ [W Hz$^{-1}$] |
|---|---|---|---|---|---|---|
| 0034+25 | 37±4 | 2.0±0.7 | 5.4±2.0 | 108±11 | 22.58 | 22.04 |
| 0326+39 | 340±17 | 11.8±2.0 | 3.5±0.6 | 118±10 | 23.31 | 22.65 |
| 0828+32 | 469±20 | 37±3.0 | 7.9±0.7 | 73±5 | 24.07 | 21.96 |
| 0844+31 | 318±12 | 7.1±1.0 | 2.2±0.3 | 20±4 | 24.13 | 23.45 |
| 0915+32 | 93±5 | 4.5±0.5 | 4.8±0.6 | 129±7 | 23.53 | 22.52 |
| 0924+30 | 10±4 | 1.7±1.1 | 17±18 | — | 21.86 | < 20.48 |
| 1116+28 | 119±13 | 4.7±1.0 | 3.9±1.2 | 88±9 | 23.69 | 23.17 |
| 1321+31 | 455±20 | 114±6 | 25±2 | 111±3 | 23.09 | 21.77 |
| 1615+35 | 395±28 | 24±1.5 | 6.0±0.6 | 48±6 | 23.54 | 22.42 |
| 1827+32 | 100±16 | 5.4±1.5 | 5.4±2.5 | 82±9 | 23.61 | 23.08 |

the secondary lobe system is brighter even at this high radio frequency (see Fig. 4a). Our map of linear polarization (Fig. 4b) shows that the north-eastern lobe of the main lobe system is about twice as bright as the south-western one; this asymmetry is also apparent at lower frequencies (see Figs. 1b and 2b of Parma *et al.* 1985), though less pronounced. The degrees of polarization in the lobes are higher than those measured at lower frequencies in spite of our poorer resolution, with ~20% in the southern extension and north-eastern lobe, and ~12% in the south-western lobe. The maximum degree of polarization occurs near the outer boundaries of the north-eastern lobe reaching ~30% there. Our polarization angles indicate that a rotation measure study involving these frequencies may be necessary, in contrary to the conclusion of Parma *et al.* (1985). This holds at least for the outer edges of the main lobes, near the hot spots, which are visible in the high-resolution maps of de Ruiter *et al.* (1986) and Fanti *et al.* (1987).

The radio spectrum (Fig. 11c) is straight, not indicating any significant steepening at the higher frequencies. This is because the secondary lobes, which do show aging effects, do not contribute significantly to the total radio power of 0828+32 at 10.6 GHz. The spectral index between 408 MHz and 10.6 GHz is $\alpha = -0.70 \pm 0.03$.

### 3.4. B2 0844+31.

This source was studied between 610 MHz and 5 GHz by van Breugel & Miley (1977), by van Breugel (1980) and by Jägers (1986) with the WSRT, and by Machalski & Condon (1985) with the VLA. Our 10.6 GHz map, shown in Figure 5a, is dominated by the emission from the lobes, whereas the central source is less pronounced. No linear polarization has been detected in the latter at this frequency, whereas the lobes are strongly polarized, the northern one up to ~25%, the southern one up to ~10% (see Fig. 5b). Given the relatively tangled magnetic field structure which is suggested by the observed distributions of polarization vectors (see van Breugel (1980) and our Figs. 5a and b) there must be significant beam depolarization with our current resolution. However, the relatively high degree of polarization seen in the northern lobe at 10.6 GHz implies Faraday depolarization, too, if compared with the 0.6 and 1.4 GHz observations of Jägers (1986). A preliminary comparison between our polarization vectors and those of van Breugel (1980) indicates a positive rotation measure across the source, with RM $\simeq 19\,\mathrm{rad\,m^{-2}}$ in the northern lobe, and RM $\simeq 25\,\mathrm{rad\,m^{-2}}$ in the southern one. This is about twice the value estimated by van Breugel, but is not conflicting with his conclusion of preferentially circumferential magnetic fields in the northern and southern lobes. In fact the above rotation measures imply that our polarization vectors are only ~1° off (anti-clock wise) from the intrinsic orientations.

The integrated spectral index derived between 408 MHz and 10.6 GHz is $\alpha = -0.75 \pm 0.02$, and the spectrum does not exhibit any sign of steepening at high radio frequencies (Fig. 11d).

### 3.5. B2 0915+32.

This source, which is associated with a galaxy pair belonging to a rather loose group, was observed at 1.4 GHz by Ekers *et al.* (1981) and at 5 GHz by Parma *et al.* (1985), using the WSRT. VLA observations at 1.435 GHz were reported by de Ruiter *et al.* (1986). Our map of this source at 10.6 GHz (Fig. 6a) suggests a total size of ~7′.5 at this frequency, somewhat less than the total size at 1.4 GHz determined by Parma *et al.* At high resolution the source exhibits a complex bending structure, reminiscent of that of 3C 31 and 3C 449, which has been interpreted in terms of interaction models (e.g. Blandford & Icke 1978). This is not unlikely in the case of 0915+32, given the proximity of two galaxies. The 10.6 GHz map does not show, however, any clear evidence for this bending structure on a large scale as is evident in the core of 3C 31 and 3C 449 (in particular in the former, see Andernach *et al.* 1992).

Our map of linear polarization (Fig. 6b) is the first to reveal the magnetic field structure in 0915+32. The polarization vectors, assuming negligible Faraday rotation, suggest that the magnetic field commences with a longitudinal orientation near the central source, while in the northern low-brightness region it could be largely perpendicular. However, this has to be checked by polarization measurements at lower frequencies as we cannot rule out Faraday rotation completely. That Faraday effects may play a role in this source is strongly suggested by the peculiar behaviour of the linearly polarized emission in the south: the observed degree of polarization increases gradually, reaching ~20–30% near the location where the polarized intensity exhibits a very sharp gradient in the south of the central bright region. This sharp cutoff is very suggestive of depolarization, which has to be investigated by incorporating lower frequencies.

The integrated radio spectrum (Fig. 11e) is straight and fairly flat between 1.4 GHz and 10.6 GHz, with $\alpha = -0.56 \pm 0.01$.

### 3.6. B2 0924+30.

This radio source, associated with the luminous E/SO galaxy IC 2476, is likely to be a relic radio galaxy in which the central engine has been switched off about $10^8$ yrs ago (Cordey, 1987). Our present observations fully corroborate this view. Our full resolution map (not shown here) does not exhibit any emission at the 2 mJy/b.a. ($2\sigma$) level in total power, or at the 1 mJy/b.a. ($2\sigma$) level in linear polarization. It is only after considerable smoothing (~2'.5) that significant emission is disclosed. We have performed a careful ring integration of the map in elliptical rings, the ellipse parameters chosen such as to fit the observed low-frequency distribution (see the maps of Ekers *et al.* 1975, 1981; Cordey, 1987). A 22 mJy source, designated 'B' by Ekers *et al.* (1975) and by Cordey (1987), was subtracted from the map prior to the integration. The total 10.6 GHz flux density of 10 mJy obtained here is quite uncertain (40% error), therefore more sensitive observations of this source will be made. Marginal polarized emission, too, was seen after smoothing, but the derived degree of linear polarization is not significant.

The integrated radio spectrum of 0924+30 is displayed in Figure 11f. Note the dramatic steepening between 1.4 and 10.6 GHz, which clearly reflects the aging of the relativistic particles. The spectral index between 1.4 and 10.6 GHz is $\alpha = -1.87 \pm 0.20$, which is steeper than that found in the low frequency range ($\alpha = -1.2$, Ekers *et al.* 1981) A high-frequency study of the spectral index as well as the polarization distribution across this "relaxed" source is compelling. To this end, a very sensitive map at 10.6 GHz is required which will be obtained in due course.

### 3.7. B2 1116+28

This WAT source was first mapped with the WSRT at 1.415 GHz by Fanti *et al.* (1978). Observations with higher sensitivity at 1.4 GHz and 5 GHz were made by Parma *et al.* (1985) using the same radio telescope. VLA observations at 1.4 GHz were reported by de Ruiter *et al.* (1986). Our total intensity map (Fig. 7a) shows the same WAT morphology as seen at lower frequencies. The polarized emission, displayed in Figure 7b, confirms the results of Parma *et al.* (1985), suggesting a magnetic field which is oriented perpendicular with respect to the jets of this source. The central component, designated 'c' by Parma *et al.* (1985), shows a polarization angle of p.a. ~ 88° in Figure 7b, while Parma *et al.* determined p.a. = 105° at 1.4 GHz. This corresponds to a rotation measure of RM $\approx 7\,\mathrm{rad\,m^{-2}}$ and is in agreement with the Faraday rotation seen by Parma *et al.* between 1.4 and 5 GHz. Their value of RM is erroneous and should be RM = $5\,\mathrm{rad\,m^{-2}}$ (instead of 21). The observed degree of polarization at 10.55 GHz is highest in the eastern lobe, exceeding 20% there. The western one shows about 15%, while the central region is ~8% polarized. All of these values are higher than those found at 1.4 GHz, indicating significant depolarization at lower frequencies, especially in the lobes. The central source shows only a slight increase of linear polarization at high frequencies.

The integrated radio spectrum of B2 1116+28 (Fig. 11b) is straight up to high frequencies, with $\alpha = -0.67 \pm 0.01$ between 408 MHz and 10.55 GHz.

### 3.8. B2 1321+31

This radio galaxy was previously studied in detail at 610 MHz, 1.4 GHz and 5 GHz by Ekers *et al.* (1981) and by Fanti *et al.* (1982). The source is relatively nearby and hence quite extended (~12'). Its most salient feature is its strong linear polarization which is seen over most of its extent (Fanti *et al.* 1982). Our map at 10.6 GHz is shown in Figure 8a which corroborates the finding of strong polarization. At 10.6 GHz, B2 1321+31 exhibits a maximum degree of polarization of ~50% in the bright inner portion of its edge-darkened morphology, but there is strong polarization essentially all over the source (see Fig. 8b). The total intensity distribution exhibits 5 maxima along the ridge line, one coincident with the central source, and two pairs of maxima about 1'.9 and 2'.9, respectively, away from the central source. These maxima are also visible at 610 MHz, except for the central source (see Fanti *et al.* 1982) indicating a rather flat spectrum of the nuclear source at low frequencies. The radio emission widens significantly towards the outer lobes, which is also evident at lower frequencies (see the 610 MHz and 1.4 GHz maps of Fanti *et al.*). The polarized intensity (Fig. 8b) shows two distinct maxima about 1'.4 away from the source centre. These maxima can be also recognized in the 1.4 GHz polarization map of Fanti *et al.* There is a prominent polarized extension visible in the south-west, in which the degree of polarization exceeds some 50%. The polarization angle shows hardly any variation, the mean value at 10.6 GHz being 111°±3°. This is entirely consistent with the results of Fanti *et al.*, indicating that the observed polarization angles at 10.6 GHz are again close to intrinsic. This, along with the similar degrees of polarization measured at both low and high frequencies, suggests that beam depolarization on scales smaller than ~10″ (~3 kpc) is the dominating process here, rather than Faraday depolarization. Otherwise, we would expect a strong wavelength dependence (Burn 1966), which is not observed. The magnetic field in B2 1321+31 must, however, be ordered on scales larger than ~10″, for we would expect stronger beam depolarization with the larger beam of the present observations. The mean degree of po-

larization is also very high, $< p >= 25 \pm 2\%$. Parma & Weiler (1981) measured ~18% with their cross-scanning technique and the beam of 4'.5 HPBW. The polarization angle they derived appears to be too high if compared with our integral value (Tab. 3) and the lower-frequency study of Fanti *et al.* (1982; see their Fig. 7).

The total radio spectrum of B2 1321+31 is rather well defined between 408 MHz and 10.6 GHz. There is no obvious steepening at higher frequencies (Fig. 11h), which may be related to the very uniform magnetic field morphology, i.e. the particles can essentially move along the field lines without losing too much energy. The integral spectral index between 408 MHz and 10.6 GHz is $\alpha = -0.64 \pm 0.01$.

### 3.9. B2 1615+35.

A 1.465 GHz VLA map of this source was published by Machalski & Condon (1985) but also by O'Dea and Owen (1985). Maps obtained with the WSRT at 0.6, 1.4 and 5 GHz were presented by Ekers *et al.* (1978). Figure 9a shows our 10.6 GHz map of this head-tail source. The head-tail structure can be also seen at this frequency, in spite of the low angular resolution. The source at $\alpha_{50} = 16^h15^m24^s.7$, $\delta_{50} = 35°15'38''$ has a spectral index of $\alpha = -0.7 \pm 0.1$ between 1.465 and 10.6 GHz. It seems very unlikely that it is related to B2 1615+35. The observed linear polarization at 10.6 GHz (Fig. 9b) shows four maxima, of which the south-eastern one coincides with the head of the source. These polarization maxima appear to be associated with maxima of the total intensity at 1.465 GHz visible in the higher-resolution map of Machalski & Condon (1985). The south-eastern one shows a steep gradient in linear polarization towards the leading edge of the source, similar to the case of B2 0915+32 (Sect. 3.5). If there is no significant Faraday rotation, the observed polarization angles suggest a magnetic field which is generally oriented along the tail. The observed degrees of polarization vary between ~10% in the head of the source and ≳30% in the north-western low-brightness end of the tail. The average degree of polarization at 10.6 GHz, $< p >= 6.0 \pm 0.6\%$, is comparable to the 5 GHz value reported by Fanti *et al.* (1981). The mean polarization angle derived at 10.6 GHz is consistent with the data at 1.4 GHz and 5 GHz (Fanti *et al.*), giving a rotation measure of RM $\approx 14\,\mathrm{rad\,m^{-2}}$.

The radio spectrum of B2 1615+35 is straight up to 10.6 GHz (Fig. 11i), the mean spectral index between 408 MHz and 10.6 GHz being $\alpha = -0.80 \pm 0.03$.

### 3.10. B2 1827+32.

The source was thoroughly observed with the VLA at 20 cm by Parma *et al.* (1985), by de Ruiter *et al.* (1986), and by Fanti *et al.* (1986). Our map of this source is displayed in Figure 10a. At 10.6 GHz the strongest emission comes from the central source (designated 'b' by Parma *et al.* 1985), while the south-western component ('c') is less prominent than at 1.4 GHz. This implies a rather flat spectrum of the nuclear source. The source is also polarized, the strongest polarized radiation featuring the same regions as found by Parma *et al.* at 1.4 GHz. The degree of polarization reaches 20–30% in some locations, which are alternating with locations of very weak polarization (see Fig. 10b). The observed degrees of polarization at 1.4 GHz are significantly lower, indicating strong depolarization at lower frequencies. A preliminary comparison of our polarization angles with those derived by Parma *et al.* yields a rotation measure of RM $\approx -16\,\mathrm{rad\,m^{-2}}$. Our polarization vectors indicate a magnetic field orientation which roughly follows the bending lobes of this source. Note, however, that the derived polarization angles have relatively large uncertainties of order 10°, owing to the weak polarized emission seen here.

The integral radio spectrum of B2 1827+32 which is shown in Figure 11j is straight again up to 10.6 GHz, with $\alpha = -0.61 \pm 0.05$ between 408 MHz and 10.6 GHz.

### 3.11. General properties of the sources.

This is the first high-frequency investigation of a large sample of low-luminosity radio galaxies which is sensitive to the large-scale structure of the total and linearly polarized radio emission of such objects. The present study incorporates 10 such radio sources whose angular sizes exceed 4'. In Table 4 we have compiled the integral source properties resulting from the present investigation. Two of the sources are edge-brightened, and eight are edge-darkened. One of these is a head-tail source, two of them are WAT sources, and one of them is a relic radio galaxy, the central engine of which was switched off long ago. In seven out of ten sources a double or single jet is present.

The monochromatic radio luminosity of the sources at 10.6 GHz (Tab. 4) covers about 2 orders of magnitude, $P_{10.6} \approx 10^{22} - 10^{24}\,W\,Hz^{-1}$, with the lowest luminosity radiated by B2 0924+30, the relic radio galaxy. A correlation between the total luminosities at 10.6 GHz and the 5 GHz core luminosities is present, with the exception of B2 0924+30. This is to be expected in view of the same correlation seen by Giovannini *et al.* (1988) at 408 MHz, suggesting a connection between the energy delivered by the central engines of the sources and their total radio power *while they are active*.

The observed degrees of linear polarization cover a range of between 5% – 30% in the different components of the sources, and it is only in B2 1321+31, which is exceptional, that we find fractions of polarization in excess of ~50%. In general, the degree of polarization in the lobes is higher (17% on average) than that in the central component (9% on average) of the sources. The degrees of po-

larization at 10.6 GHz are significantly higher on average than those measured at lower frequencies (e.g. 1.4 GHz), in spite of our comparably low angular (and hence spatial) resolution. This wavelength dependence shows that apart from beam depolarization effects, also Faraday depolarization has to be considered.

A preliminary analysis of the measured polarization angles indicates low rotation measures ($|$ RM $| \lesssim 20\,\mathrm{rad\,m^{-2}}$) so that at 10.6 GHz we essentially map the intrinsic (projected) magnetic field orientations. Our data show that the overall magnetic field orientation is parallel to the jet axes in the inner parts of the sources in 4 cases, and perpendicular to it in 5 cases. In these latter 5 cases the part of the source with perpendicular magnetic field corresponds in higher resolution maps to a region where a double jet is visible. In B2 0844+31 the internal longitudinal magnetic field traces the one sided jet region. In the lobes the magnetic field is always tangential to the edges, as already seen in a number of sources at lower frequency (Bridle *et al.* 1991). In B2 1615+35, the only NAT source present in the sample, the magnetic field closely follows the orientation of the tail.

Except for B2 0924+30, none of the sources studied here show any sign of significant particle aging in their integrated radio spectra, i.e. there are no signs of any steepening towards 10.6 GHz. These should show up though in the spectral index distributions that can be derived from the maps presented here, if compared in detail with the low-frequency investigations. Such a point-by-point comparison, which will also provide accurate studies of the depolarization and Faraday rotation across the sources, will be presented elsewhere.

## 4. Summary and conclusions.

We have mapped a sample of 10 B2 low-luminosity radio galaxies at 10.6 GHz using the new 4-horn receiver system installed in the Effelsberg 100-m telescope. For the first time, the large-scale distribution of the total and linearly polarized radio emission has been sensitively measured for a larger sample of low luminosity sources. The present study allows the following preliminary conclusions:

1. The 10.6 GHz emission extends over scales which are comparable to the source sizes observed at lower frequencies.
2. In three cases the flat spectrum cores of the sources are rather pronounced at 10.6 GHz.
3. The total monochromatic radio luminosity at 10.6 GHz is correlated with the 5 GHz core luminosity of the sources.
4. The observed degrees of linear polarization in the lobes are higher on average than those measured in the central components, the latter encompassing the core and inner jet regions.
5. The degrees of polarization are higher at 10.6 GHz than what is measured at lower frequencies, hinting at significant Faraday depolarization, considering the relatively large beam size ($\sim 1'$) involved in the observations presented here.
6. At 10.6 GHz the observed polarization angles are essentially intrinsic (to within $\lesssim 2°$).
7. It appears that the magnetic field orientation is related to the morphology of the source: it is perpendicular in the double jets, longitudinal in the one sided jet and tails, and longitudinal in the lobes.
8. No significant steepening of the high-frequency integrated radio spectrum is found except in one case, B2 0924+30, which is known to be a relic radio galaxy.

The measurements presented here must be regarded as a pilot study which will be pursued by observing larger source samples of this kind. More detailed comparisons with low-frequency data will be presented elsewhere, which will allow very accurate determinations of the spectral index, rotation measure and depolarization characteristics across the sources, and thus provides an important diagnostic tool to investigate the thermal and nonthermal properties of the material in radio galaxies.

## References

Andernach H., Feretti L., Giovannini G., Klein U., Rosetti E., Schnaubelt J. 1992, A&A (in press)
Baars J.W.M., Genzel R., Pauliny-Toth I.I.K., Witzel A. 1977, A&A 61, 99
Blandford R.D., Icke V. 1978, MNRAS 169, 395
Bridle A.H., Baum S.A., Fomalont E.B. *et al.* 1991, A&A 245, 371
Burn B.J. 1966, MNRAS 133, 67
Colla G., Fanti C., Fanti R. *et al.* 1975, A&AS 20, 1
Cordey R.A. 1987, MNRAS 227, 695
de Ruiter H.R., Parma P., Fanti C., Fanti R. 1986, A&AS 65, 11
de Ruiter H.R., Parma P., Fanti C., Fanti R. 1990, A&A 227, 351
Ekers R.D., Fanti R., Lari C., Ulrich M.-H. 1975, Nat 258, 584
Ekers R.D., Fanti R., Lari C., Ulrich M.-H. 1978, A&A 69, 253
Ekers R.D., Fanti R., Lari C., Parma P., 1981, A&A 101, 194
Emerson D.T., Gräve R. 1988, A&A 190, 353
Emerson D.T., Klein U., Haslam C.G.T. 1979, A&A 76, 92
Fanti C., Fanti R., de Ruiter H.R., Parma P. 1986 A&AS 65, 145
Fanti C., Fanti R., de Ruiter H.R., Parma P. 1987, A&AS 69, 57
Fanti R., Gioia I.M., Lari C., Ulrich M.-H. 1978, A&AS 34, 341

Fanti R., Lari C., Parma P. *et al.* 1982, A&A 110, 169
Fanti R., Lari C., Parma P., Ekers R.D. 1981, A&A 94, 61
Feretti L., Dallacasa D., Giovannini G., Venturi T. 1990, A&A 232, 337
Gioia I.M., Gregorini L., Klein U. 1982, A&A 116, 164
Giovannini G., Feretti L., Gregorini L., Parma P. 1988, A&A 199, 73
Haslam C.G.T. 1974, A&AS 15, 333
Jägers W.J. 1986, Ph.D. Thesis. University of Leiden
Klein U., Emerson D.T. 1981, A&A 94, 29
Kronberg P.P., Wielebinski R., Graham D. 1986, A&A 169, 63
Machalski J., Condon J.J. 1985, AJ 90, 5
Morganti R., Fanti C., Fanti R., Parma P., de Ruiter H.R. 1987, A&A 183, 203
Morsi H.W., Reich W. 1986, A&A 163, 313
O'Dea C.P., Owen F.N. 1985, AJ 90, 927
Ott M., 1991, Diploma Thesis. University of Bonn
Parma P., Weiler K.W. 1981, A&A 96, 412
Parma P., Ekers R.D. Fanti R. 1985, A&AS 59, 511
van Breugel W.J.M. 1980, A&A 81, 275
van Breugel W.J.M., Miley G.K. 1977, Nat 265, 315

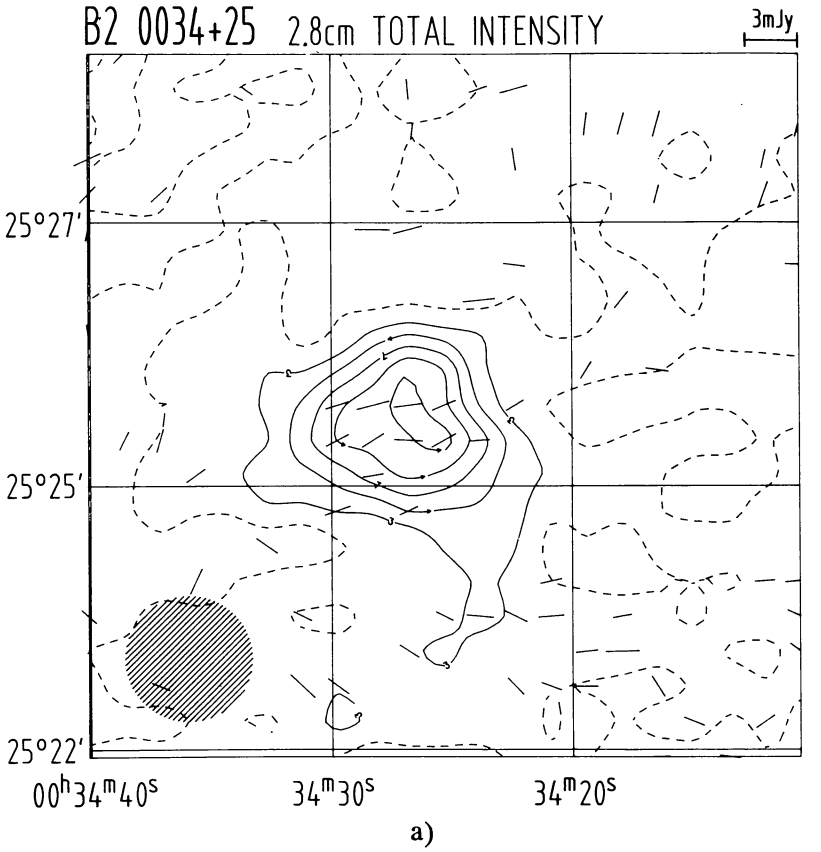


a)

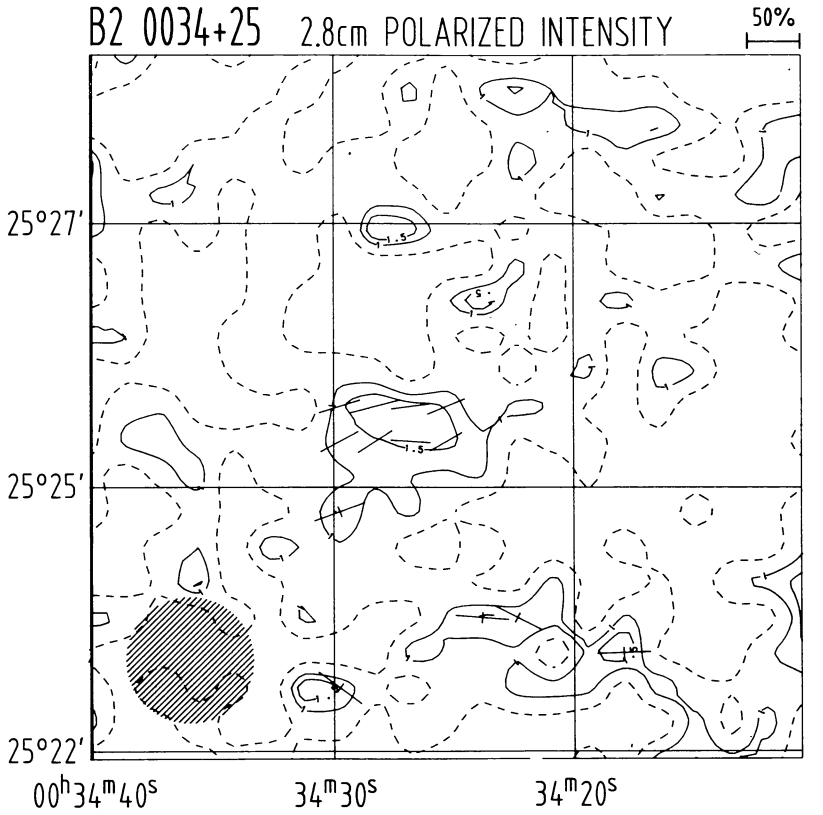


b)

FIGURE 2. 10.6 GHz map of the total (a) and polarized (b) emission of B2 0034+25.

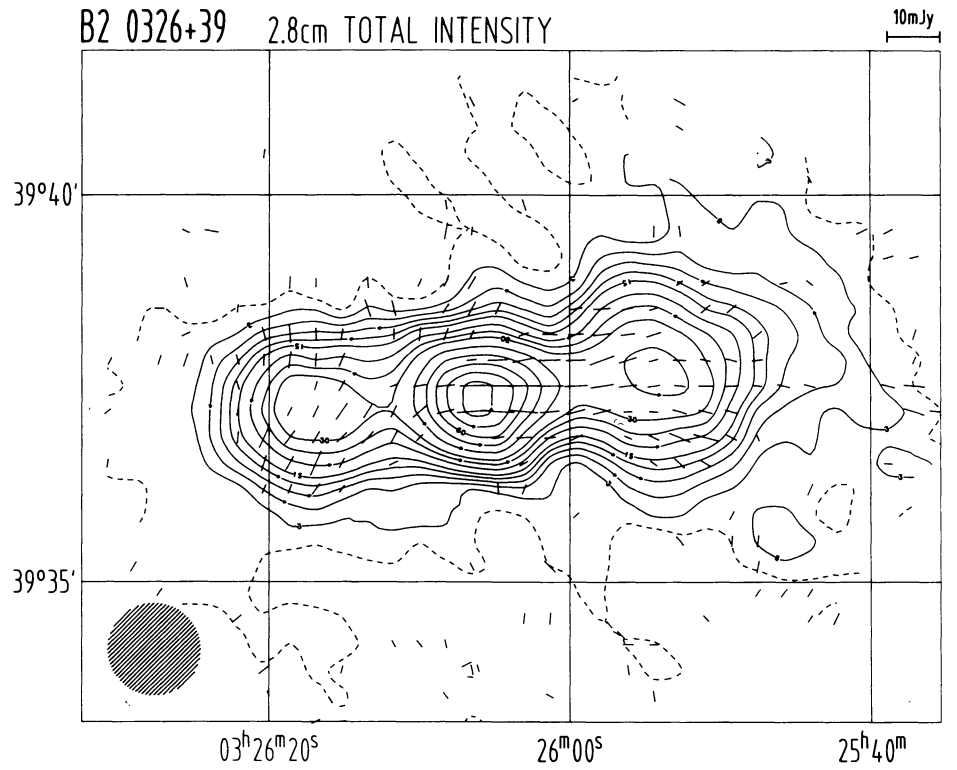


a)

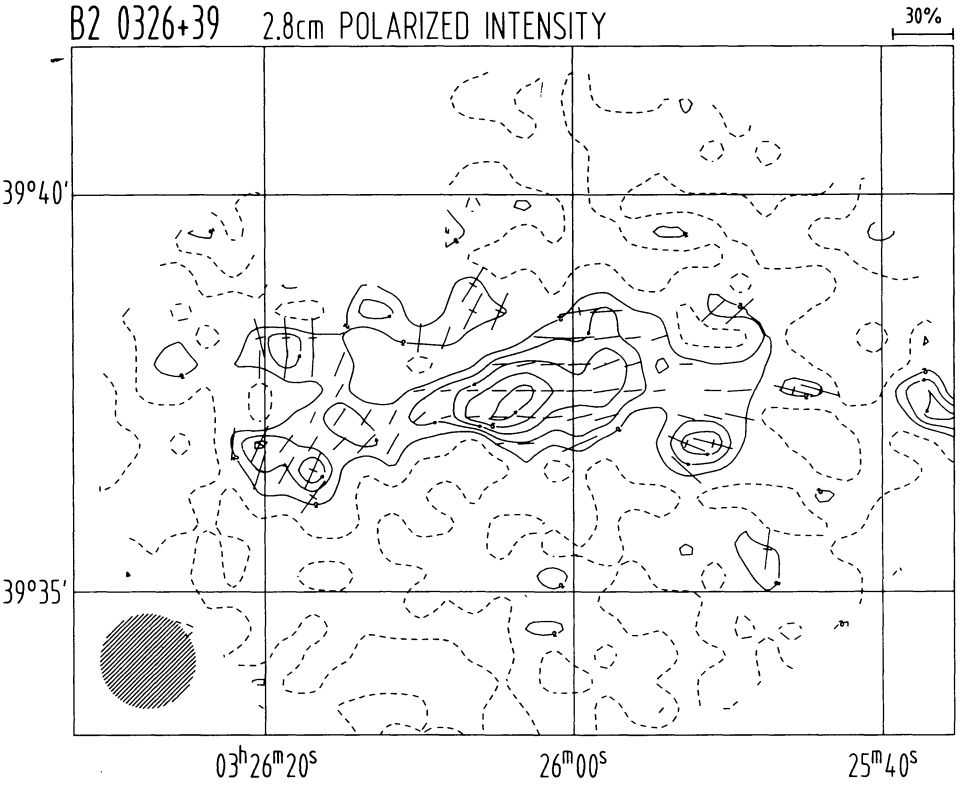


b)

FIGURE 3. 10.6 GHz map of the total (a) and polarized (b) emission of B2 0326+39.

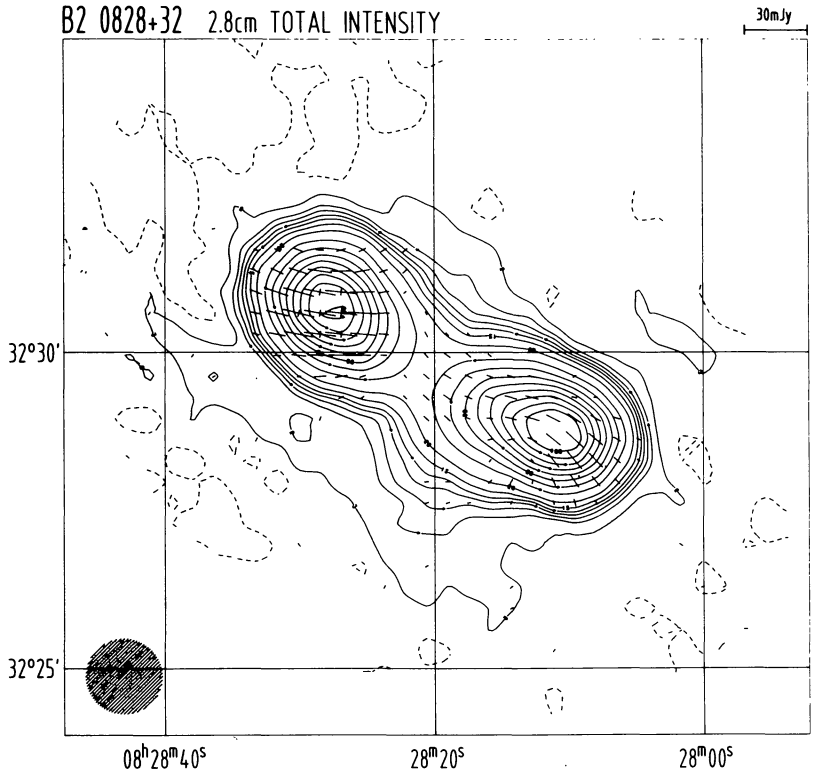


a)

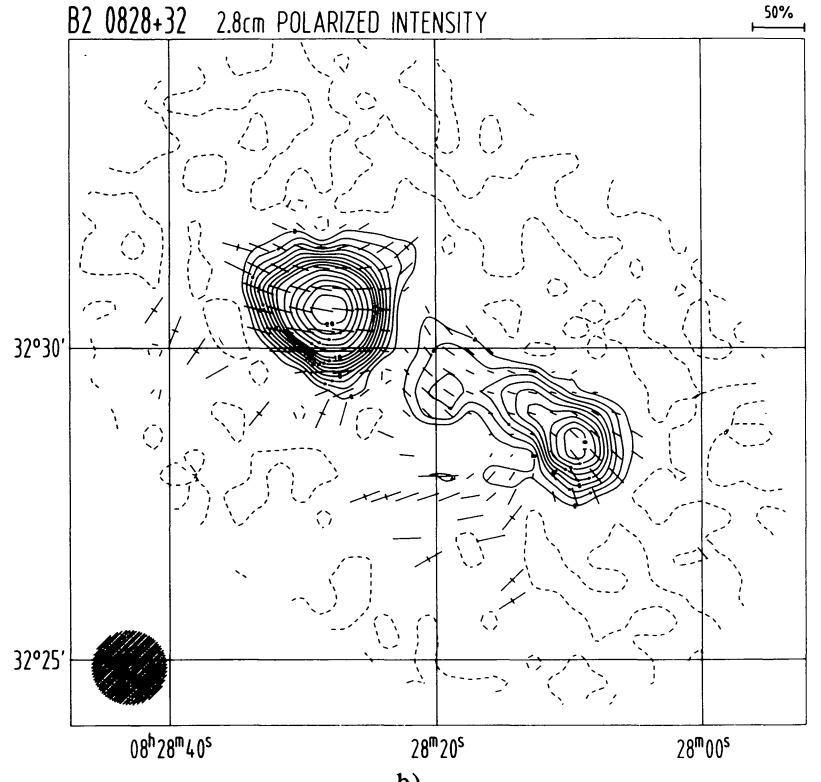


b)

FIGURE 4. 10.6 GHz map of the total (a) and polarized (b) emission of B2 0828+32.

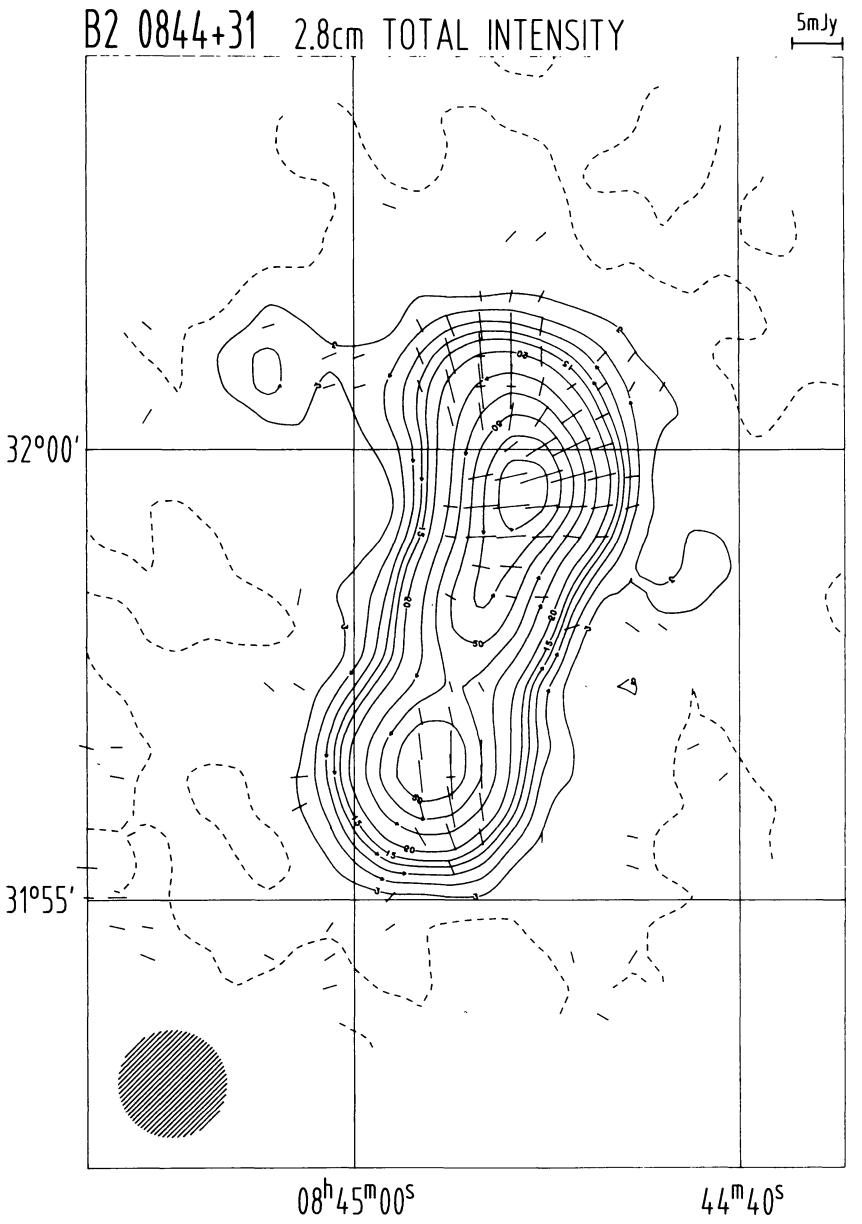


a)

FIGURE 5. 10.6 GHz map of the total (a) and polarized (b) emission of B2 0844+31.

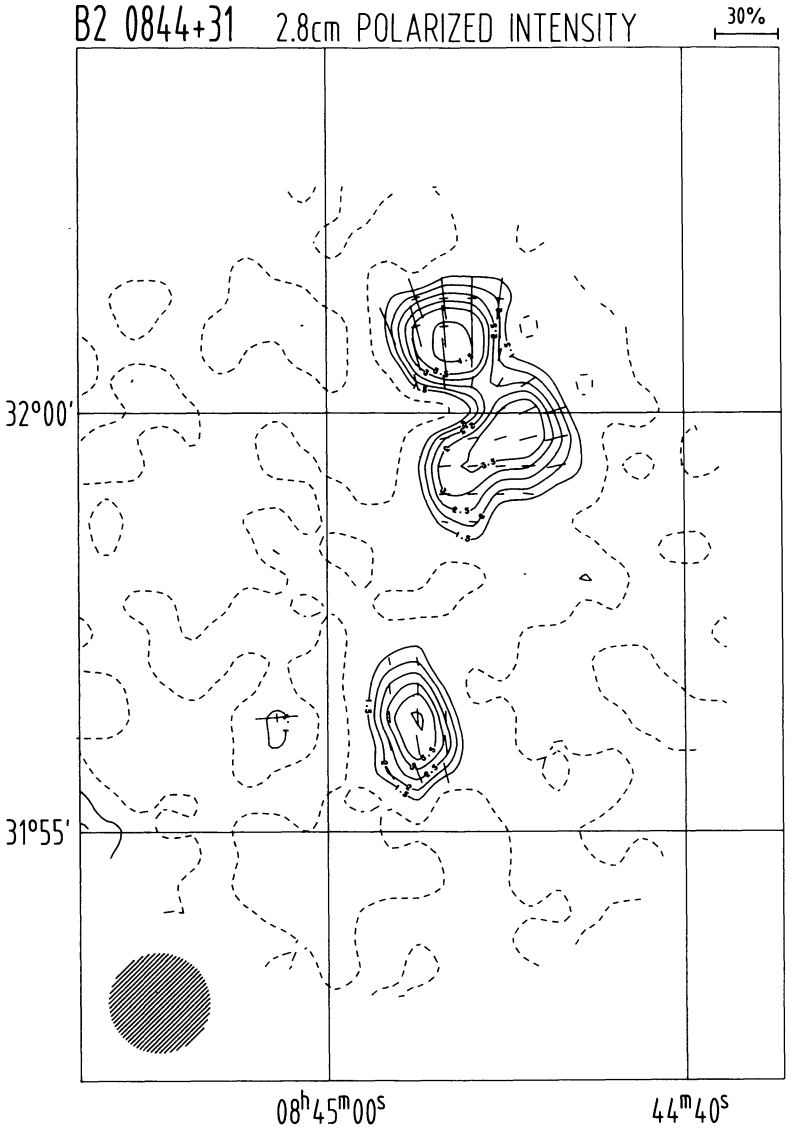


FIGURE 5b.

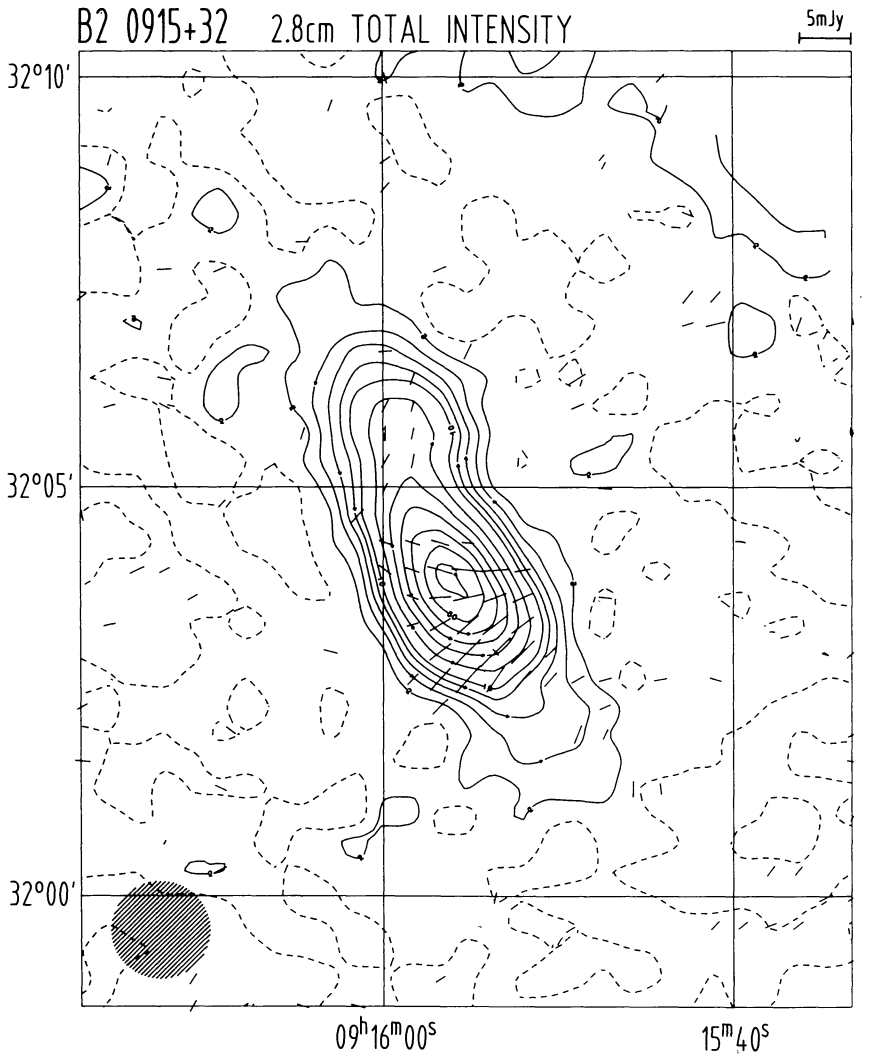


a)

FIGURE 6. 10.6 GHz map of the total (a) and polarized (b) emission of B2 0915+32.

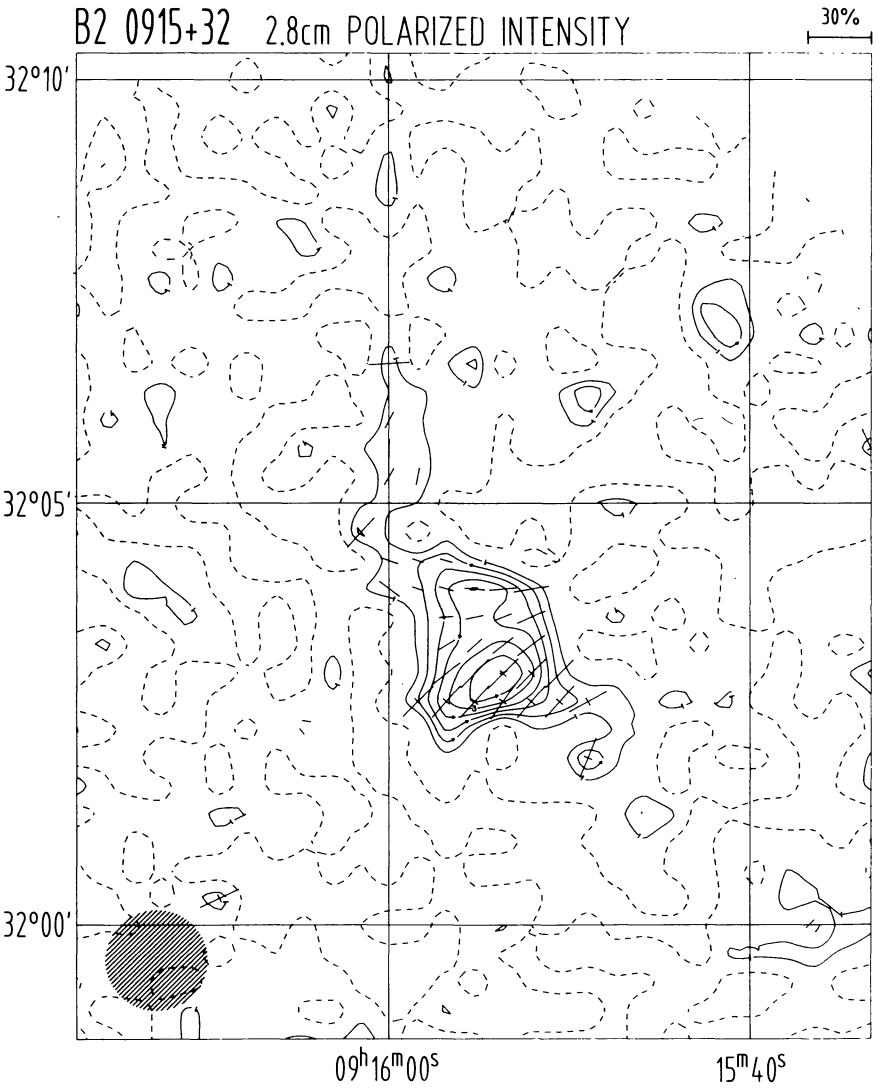


FIGURE 6b.

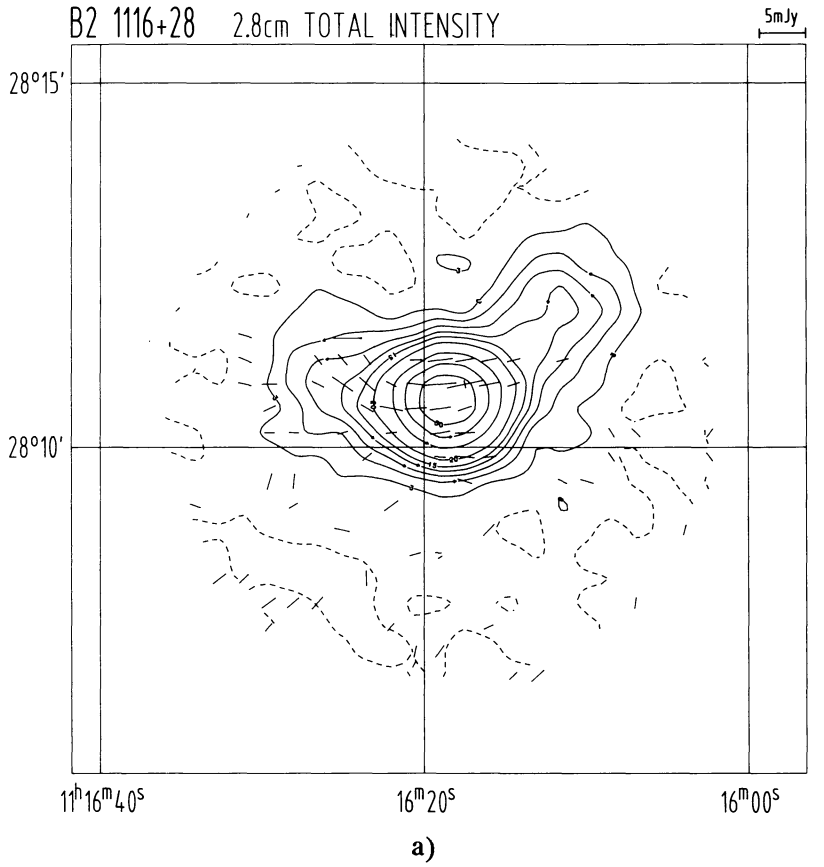


a)

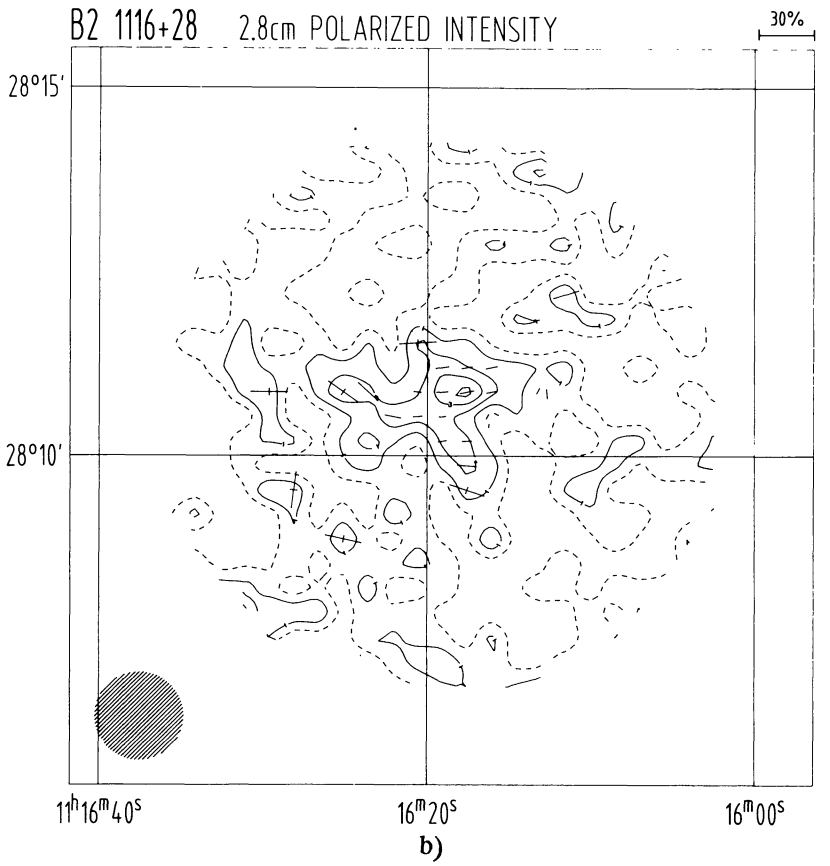


b)

FIGURE 7. 10.6 GHz map of the total (a) and polarized (b) emission of B2 1116+28.

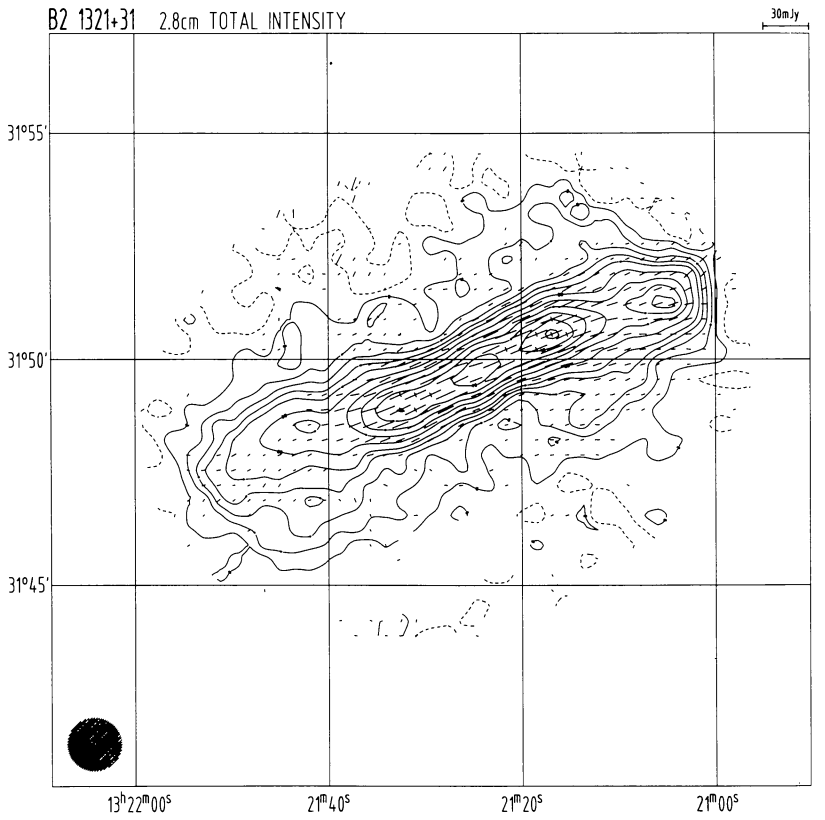


a)

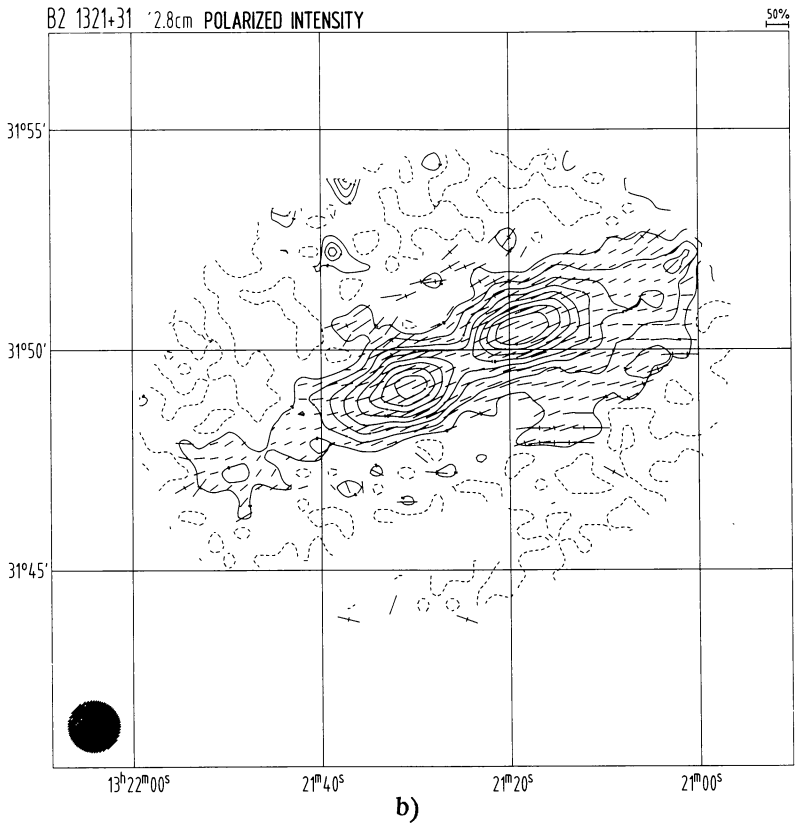


b)

FIGURE 8. 10.6 GHz map of the total (a) and polarized (b) emission of B2 1321+31.

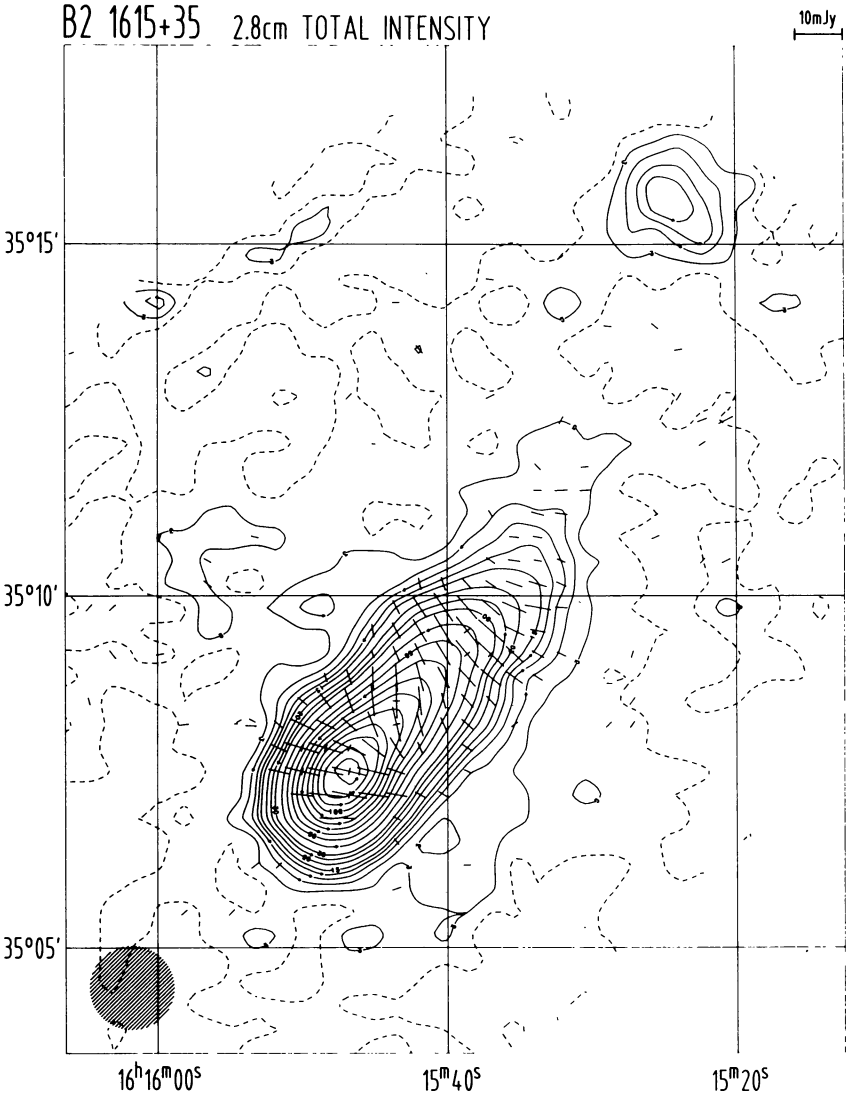


a)

FIGURE 9. 10.6 GHz map of the total (a) and polarized (b) emission of B2 1615+35.

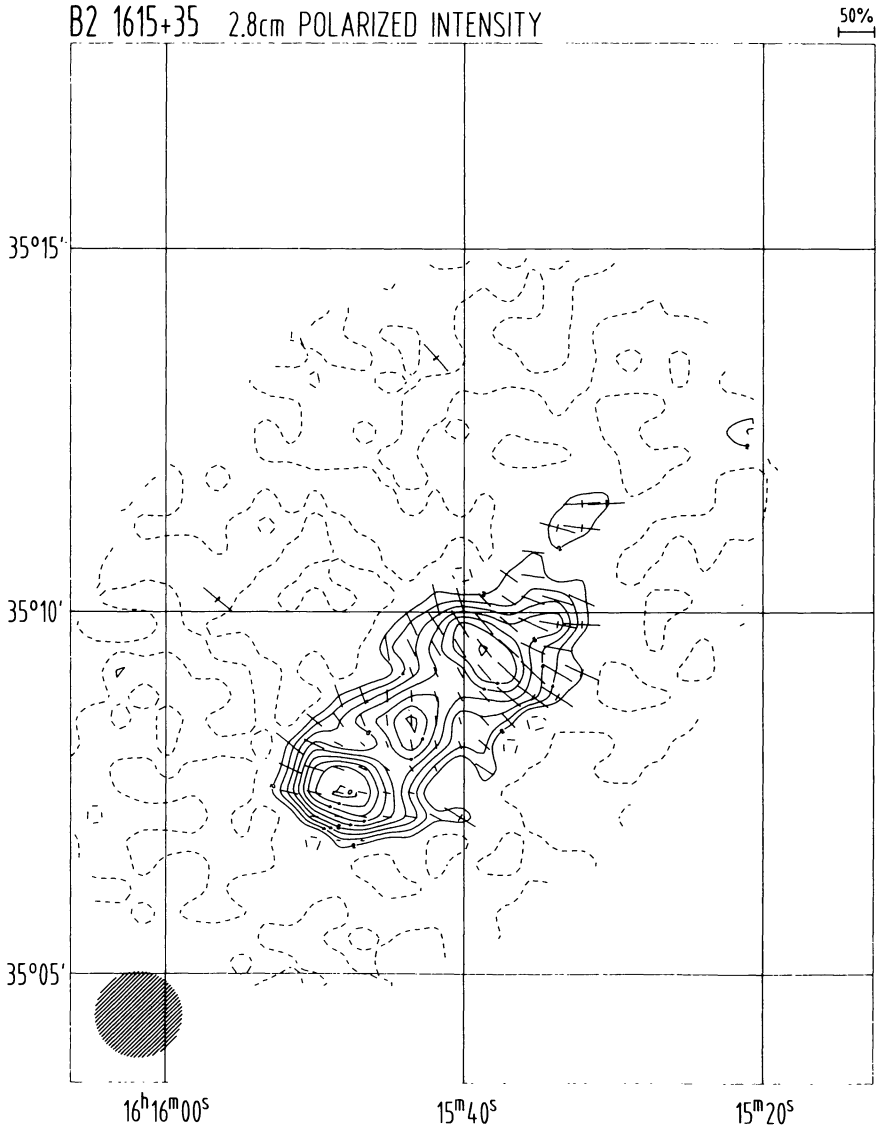


FIGURE 9b.

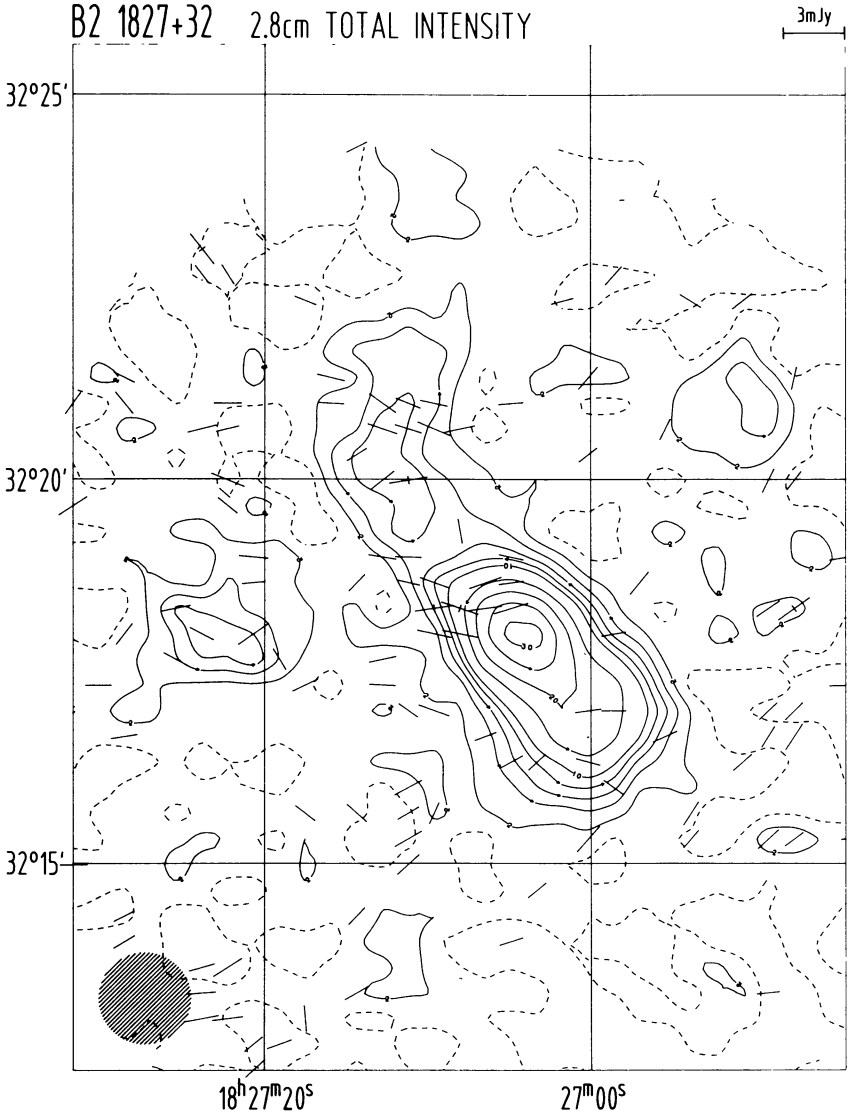


a)

FIGURE 10. 10.6 GHz map of the total (a) and polarized (b) emission of B2 1827+32.

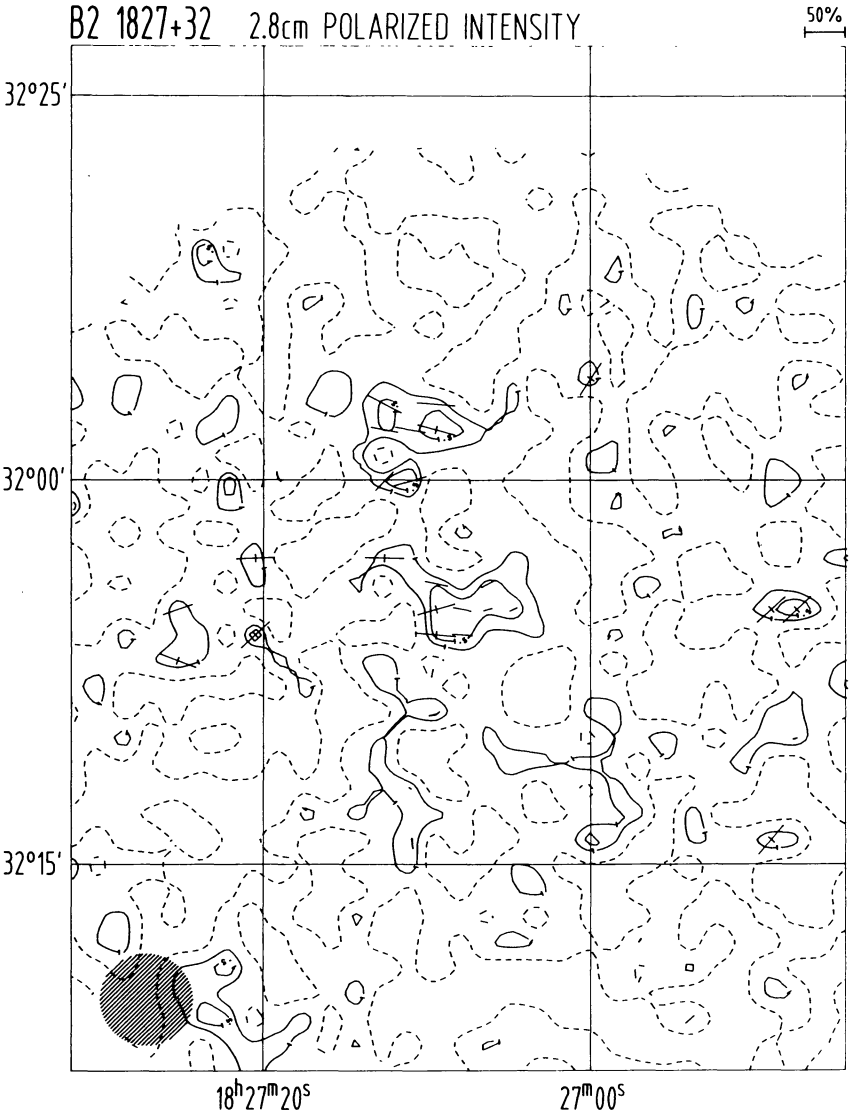


FIGURE 10b.

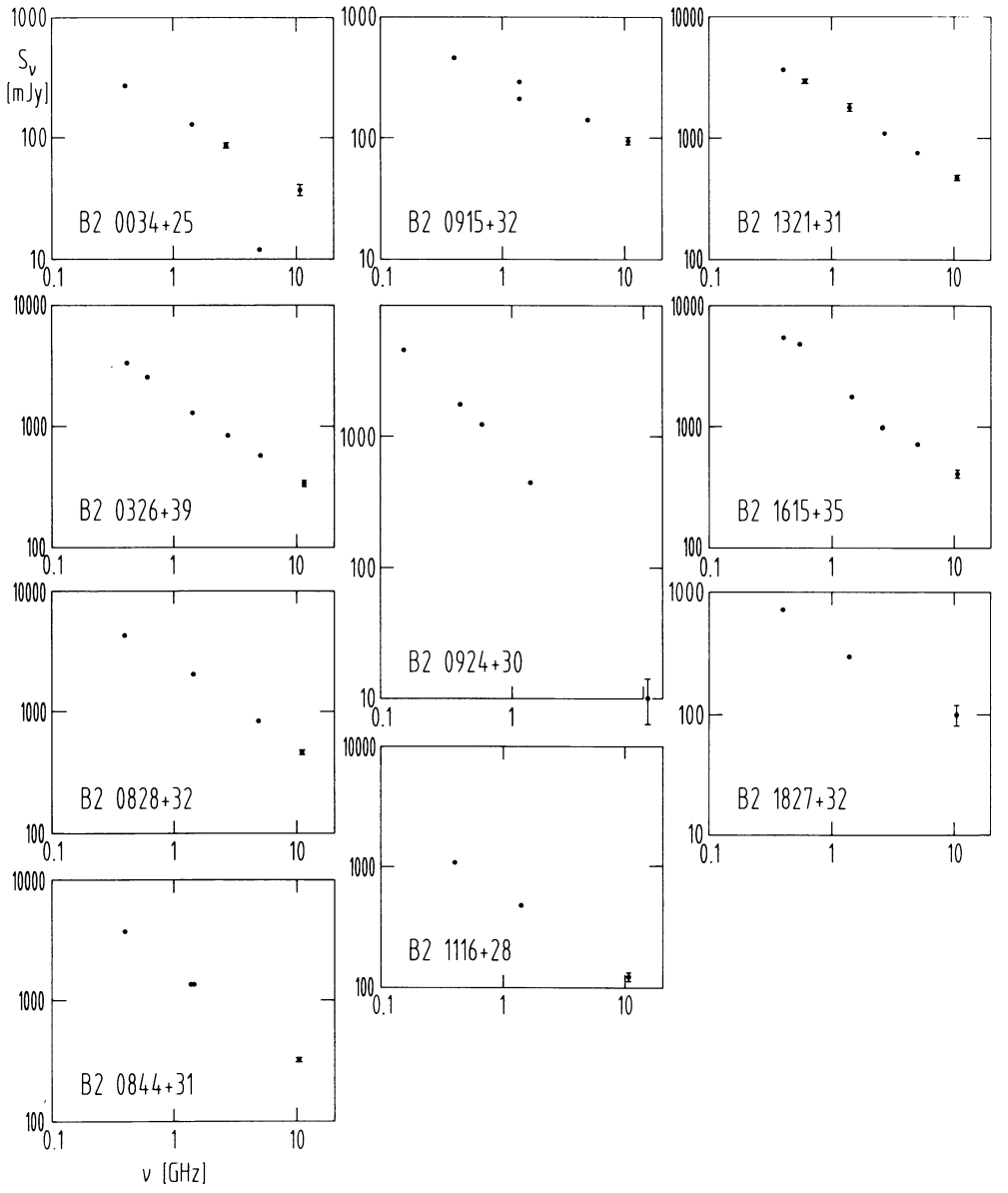


FIGURE 11. Radio continuum spectra of the B2 sources observed in the present paper (see text).